Journal of Pathology
J Pathol 2012; **226:** 108–119
Published online 26 September 2011 in Wiley Online Library (wileyonlinelibrary.com) DOI: 10.1002/path.2978

ORIGINAL PAPER

Hsa-miR-375 is differentially expressed during breast lobular neoplasia and promotes loss of mammary acinar polarity

Orsi Giricz[2], Paul A Reynolds[3], Andrew Ramnauth[1], Christina Liu[1], Tao Wang[1], Lesley Stead[4], Geoffrey Childs[5], Thomas Rohan[1], Nella Shapiro[4], Susan Fineberg[4,5], Paraic A Kenny[2]* and Olivier Loudig[1,5]*

[1] *Department of Epidemiology and Population Health, Albert Einstein College of Medicine, Bronx, NY, USA*
[2] *Department of Developmental and Molecular Biology, Albert Einstein College of Medicine, Bronx, NY, USA*
[3] *Medical and Biological Sciences Building, School of Medicine, University of St Andrews, St Andrews, UK*
[4] *Montefiore Medical Center, Bronx, NY, USA*
[5] *Department of Pathology, Albert Einstein College of Medicine, Bronx, NY, USA*

**Correspondence to: Paraic A Kenny, Department of Developmental and Molecular Biology, Albert Einstein College of Medicine, Bronx, NY, USA. e-mail: paraic.kenny@einstein.yu.edu*
**Correspondence to: Olivier Loudig, Departments of Epidemiology and Population Health, and Pathology, Albert Einstein College of Medicine, Bronx, NY, USA. e-mail: olivier.loudig@einstein.yu.edu*

Abstract

Invasive lobular carcinoma (ILC) of the breast, characterized by loss of E-cadherin expression, accounts for 5–15% of invasive breast cancers and it is believed to arise via a linear histological progression. Genomic studies have identified a clonal relationship between ILC and concurrent lobular carcinoma *in situ* (LCIS) lesions, suggesting that LCIS may be a precursor lesion. It has been shown that an LCIS diagnosis confers a 15–20% risk of progression to ILC over a lifetime. Currently no molecular test or markers can identify LCIS lesions likely to progress to ILC. Since microRNA (miRNA) expression changes have been detected in a number of other cancer types, we explored whether their dysregulation might be detected during progression from LCIS to ILC. Using the Illumina miRNA profiling platform, designed for simultaneous analysis of 470 mature miRNAs, we analysed the profiles of archived normal breast epithelium, LCIS lesions found alone, LCIS lesions concurrent with ILC, and the concurrent ILCs as a model of linear histological progression towards ILC. We identified two sets of differentially expressed miRNAs, the first set highly expressed in normal epithelium, including hsa-miR-224, -139, -10b, -450, 140, and -365, and the second set up-regulated during lobular neoplasia progression, including hsa-miR-375, -203, -425-5p, -183, -565, and -182. Using quantitative RT-PCR, we validated a trend of increasing expression for hsa-miR-375, hsa-miR-182, and hsa-miR-183 correlating with ILC progression. As we detected increased expression of hsa-miR-375 in LCIS lesions synchronous with ILC, we sought to determine whether hsa-miR-375 might induce phenotypes reminiscent of lobular neoplasia by expressing it in the MCF-10A 3D culture model of mammary acinar morphogenesis. Increased expression of hsa-miR-375 resulted in loss of cellular organization and acquisition of a hyperplastic phenotype. These data suggest that dysregulated miRNA expression contributes to lobular neoplastic progression.

Keywords: lobular carcinoma; microRNA; acinar morphogenesis

Received 13 April 2011; Revised 4 July 2011; Accepted 23 July 2011

No conflicts of interest were declared.

Introduction

Invasive lobular carcinoma (ILC) comprises approximately 5–15% of invasive breast cancer cases and various studies report 5-year average survival rates between 68% and 87% [1]. Stage at diagnosis has a pronounced effect, with a 5-year disease-specific survival rate of 98% in patients with T1N0 ILC and 72% in patients with T3N1 disease [2]. A spectrum of precursor lesions, termed lobular intra-epithelial neoplasia, has been defined, and they include atypical lobular hyperplasia and lobular carcinoma *in situ* (LCIS), characterized by several variants [3]. Genomic studies using archived specimens of LCIS found synchronously with ILC have shown a high degree of homology in chromosomal imbalances between these two lesions [4–6], indicating a clonal relationship between them, and further suggesting that LCIS may act as a precursor lesion of ILC. Molecular analyses have also revealed identical E-cadherin mutations in synchronous LCIS and ILC lesions [7].

The recognized variants of LCIS include classical LCIS, pleiomorphic LCIS, and LCIS with comedo necrosis [8–10]. While classical and pleiomorphic LCIS are E-cadherin-negative, they exhibit important differences in their immunophenotypes. Classical LCIS

has a low proliferative rate (low Ki67), is typically oestrogen receptor-positive (and progesterone receptor-positive), and rarely shows HER2 overexpression or p53 mutation. Pleiomorphic LCIS typically has a higher proliferative rate (high Ki67), may be hormone receptor-negative, and may show p53 mutation and/or HER2 overexpression [8,10,11]. LCIS is frequently multifocal and bilateral, and a biopsy finding of LCIS is associated with an increased risk of invasive breast cancer of 10–20% over 15–20 years [12,13].

The pathogenesis of LCIS and ILC and the factors promoting progression along this lineage remain poorly understood and while the majority of LCIS lesions do not progress to ILC, no biomarkers are available to distinguish high- and low-risk lesions. We propose that comparing LCIS lesions found synchronously with ILC with LCIS lesions from patients without concurrent ILC will help to identify mechanism(s) and biomarkers associated with progression of LCIS to ILC.

Recent studies have shown that the genes coding for microRNAs (miRNAs) are frequently located in cancer-associated genomic regions or in fragile sites and their aberrant expression might contribute to the development and progression of cancer [14,15]. MiRNAs are non-coding RNA molecules, 18–24 nucleotides in length, that regulate the translation and degradation of target mRNAs through base pairing in the 3′ untranslated regions (UTRs). MiRNA genes can be found either as individual or clustered genes in the genome or as embedded sequences within functional genes, in introns or in exons [16]. To date, more than 1000 human miRNAs have been identified, and studies have shown that miRNAs can bind multiple mRNA transcripts and regulate several pathways involving development, cellular proliferation and differentiation, adhesion, migration, invasion, apoptosis, and many other biological processes relevant to cancer development and progression [17]. MiRNA expression studies in breast cancer have demonstrated that miRNAs can act as tumour suppressors or as oncogenes [18,19].

In this study, we have examined the potential role of miRNAs in the progression from normal mammary tissue, through LCIS, to ILC. We performed high-throughput miRNA profiling on normal, LCIS, and ILC specimens to determine whether miRNAs may be dysregulated during neoplastic progression of this disease and specifically analysed the expression of hsa-miR-375 and its contribution to mammary epithelial architecture.

Materials and methods

Human specimens

Thirty-one archived specimens were obtained from Montefiore Medical Center (MMC), Bronx, NY, USA, after approval of the study by the Institutional Review Board. These specimens included two normal breast specimens [frozen and matched 1-month-old formalin-fixed, paraffin-embedded (FFPE)], five normal lobular breast tissues, seven specimens containing LCIS lesions alone, eight containing LCIS lesions synchronous with ILC, eight matched specimens containing ILC lesions, and one ILC found alone. The ILC specimens were all confirmed by negative E-cadherin staining. One normal pancreas was used for *in situ* hybridization analysis.

Histology and immunohistochemistry

Twelve sections were obtained from each archived breast specimen (1 to 3 years old), the first and last being haematoxylin and eosin (H&E)-stained slides, and ten intermediate 10 μm unstained sections. Lesions were identified on H&E slides and used as guides for macrodissection on unstained slides. E-cadherin immunohistochemistry was performed using the Zymed® antibody clone 4A2C7 (Zymed/Invitrogen, Carlsbad, CA, USA), following the manufacturer's instructions, at the MMC pathology laboratory.

RNA extraction and quantification

RNA from the frozen sample was extracted using TRIzol (Invitrogen Carlsbad, CA, USA). RNA from archived breast specimens was extracted using a previously described method [20]. For qRT-PCR, all RNA samples were extracted using the High Pure RNA paraffin kit (Roche Applied Science Mannheim, Germany), following the manufacturer's instructions. Total RNA was quantified on a Nanodrop ND-2000 spectrophotometer and analysed on a Bioanalyzer mRNA Nanochip (Agilent Santa Clara, CA, USA).

MiRNA expression profiling

These experiments were performed using the miRNA profiling kit from Illumina (San Diego, CA, USA) on a Sentrix® Array Matrix (96 samples) for simultaneous analysis of 735 probes (470 mature miRNAs) with input of 200 ng of total RNA, for each sample, according to the manufacturer's instructions [21]. Arrays were scanned on a BeadArray reader (Illumina) and raw data were obtained from Beadstudio (3.3).

Reverse transcription (RT) and PCR quantifications

Taqman® miRNA primers, a miRNA reverse transcription kit, and universal PCR master mix, No AmpErase® UNG [Applied Biosystems (AB), Foster City, CA, USA] were used for these experiments. Individual RT reactions using 10 ng of total RNA were assembled in PCR tubes following the manufacturer's instructions (AB). PCR quantifications were monitored on a StepOnePlus instrument (AB) and comparative thresholds were determined by averaging the results of triplicate reactions. Both RNU44 and RNU6B were used as endogenous controls for data normalization. The ΔC_t of each miRNA was determined by subtracting the

mean C_t value of RNU44 and RNU6B from the C_t value of each miRNA. The $\Delta\Delta C_t$ for each miRNA in each sample was determined by subtracting the ΔC_t of the control samples (mean of ΔC_t of five normal samples) from the ΔC_t of the samples of interest. The fold-change differences were calculated using the $2^{(\Delta\Delta Ct)}$ formula.

In situ hybridization (ISH)

These experiments were performed, following the procedure described by Jorgensen *et al* [22], using a 20 min proteinase K treatment of the sections and Exiqon double-DIG miRCURYLNA probes including a Scramble-miR, hsa-miR-375 at 40 nM, and a double-DIG miRCURYLNA U6 probe at 20 nM. Incubations were performed in array chambers in a water bath.

Cell lines and maintenance

Non-tumourigenic breast epithelial MCF-10A cells were cultured in DMEM/F12 (Cellgro-Mediatech, Manassas, VA, USA), supplemented with 5% horse serum (Invitrogen), hydrocortisone (0.5 µg/ml), mouse epidermal growth factor (EGF; 20 ng/ml), insulin (10 µg/ml), and cholera toxin (100 ng/ml; Sigma, St Louis, MO, USA), at 37 °C in a humidified incubator (5% CO_2). Human primary miR-375 (pri-miR-375) and a non-silencing control miRNA were stably and separately expressed in MCF-10A cells by lentiviral gene transfer using the pLemiR expression system (ThermoFisher Scientific, Waltham, MA, USA). The pLemiR constructs expressed Red Fluorescent protein- TurboRFP (Evrogen, Moscow, Russia) and a puromycin resistance selectable marker. Stable populations were obtained by selection with puromycin (2.5 g/ml; MP Biomedicals, Santa Ana, CA, USA) and detection of TurboRFP.

Immunofluorescence staining and confocal microscopy of MCF-10A acini

Trypsinized single cell suspensions of MCF-10A cells were seeded on top of growth factor-reduced Matrigel (BD Biosciences, San Jose, CA, USA) at 2% (without EGF) with growth medium (replaced every 3–4 days), at a density of 2900 per cm^2 [24]. Immunostaining was carried out as described by Debnath *et al* [23]. In short, the acini were fixed in Matrigel with 4% paraformaldehyde (20 min at room temperature) and permeabilized with Triton X-100 (0.5% in PBS, 10 min at 4 °C). After three washes with glycine (100 mM in PBS), primary blocking was carried out for 2 h at room temperature in PBS containing 0.1% BSA, 0.2% Triton X-100, 0.05% Tween-20, and 10% goat serum. A secondary block was carried out for 45 min at room temperature using the same blocking buffer with the addition of goat anti-mouse $F(ab')_2$ fragment (20 µg/ml; Jackson ImmunoResearch, West Grove, PA, USA). The samples were incubated with 1 : 100 anti-CD49f (α6-integrin from BD Biosciences) in full secondary block buffer overnight at 4 °C. The AlexaFluor-conjugated secondary antibody (Invitrogen) was used at 1 : 200 dilution in full primary block buffer for 1 h at room temperature. The nuclei were counterstained with Hoechst 33 342 (1 mM) for 15 min at room temperature. Confocal analyses were performed with a Leica TCS SP2 AOBS confocal microscope (Leica, Mannheim, Germany) with a 25× oil immersion objective.

Data analysis

Raw data files were imported into Partek Genomics Suite (6.5). The Partek Batch Remover tool (an ANOVA-based method) was used to control for batch effect; data were quantile normalized and analysed using ANOVA to identify miRNAs differentially expressed between neoplastic and normal specimens. For qRT-PCR experiments, p values testing for trend between the four groups were obtained by linear regression and are presented as inset box plots (Figure 3). By including an ordered variable, based on the cancer groups (group 1: normal; group 2: LCIS alone; group 3: LCIS synchronous with ILC; group 4: the synchronous ILCs) in the model as a continuous variable, the test performed on the coefficient is equivalent to a test for a linear increase of hsa-miR-375, -182, and -183 expression (ΔC_t values) across the four groups [23,25].

GEO data submission: microRNA profiling raw data and normalized data have been submitted to and posted on the GEO website (http://www.ncbi.nlm.nih.gov/geo/query/acc.cgi?acc=GSE28514).

Results

Histological presentation of lobular neoplasia

Figure 1 displays one specimen with normal lobular epithelium, one classical lobular carcinoma *in situ* (LCIS) found alone without the presence of an invasive breast cancer (LCISa), one pleiomorphic LCIS with necrosis found synchronously with an invasive lobular carcinoma (ILC) (LCISs), and the synchronous ILC (ILCs) from the same patient. As loss of E-cadherin expression is a defining feature of lobular neoplasia [11], its immunodetection was used to distinguish normal lobules from neoplastic counterparts (Figure 1, left column of panels). Regions of interest were identified from H&E-stained slides (Figure 1, centre column of panels) and carefully dissected on unstained sections (Figure 1, right column of panels).

MiRNA expression profiling of lobular neoplasia

To determine the distribution of miRNAs in normal breast epithelial cells and at successive stages of lobular neoplastic progression, we performed high-throughput profiling of 735 probes (corresponding to

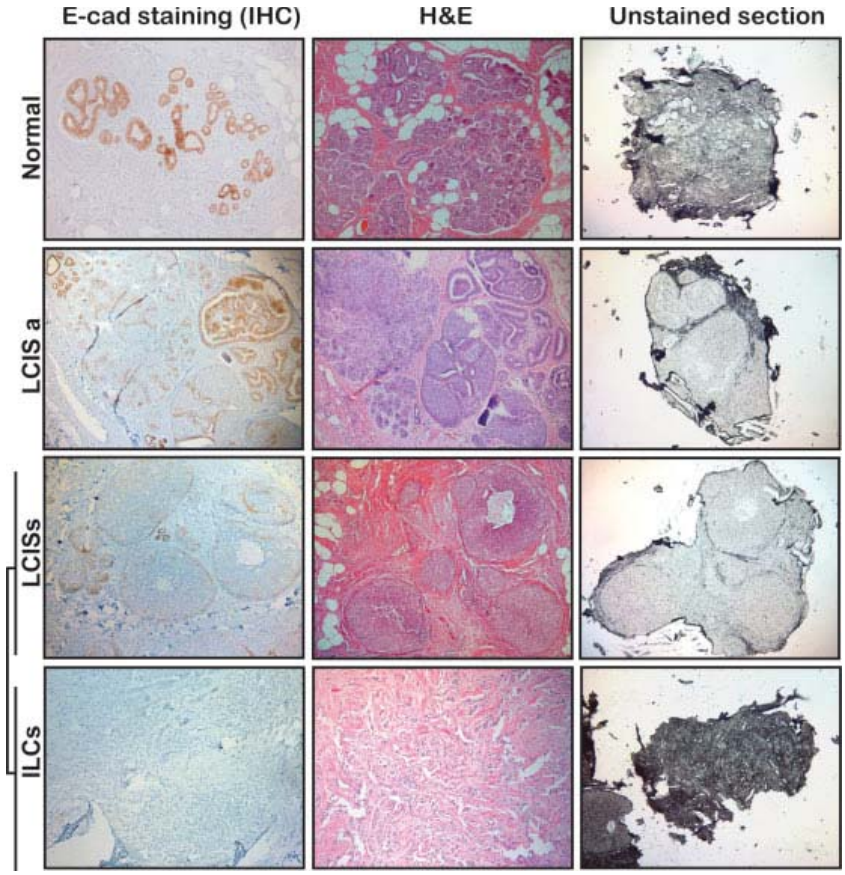

Figure 1. Microdissection of paraffin-embedded lobular neoplasia samples for microRNA analysis. Representative images of specimens used in this study. Left panels: loss of E-cadherin immunohistochemical staining was used to diagnose lobular neoplasia. Middle panels: 10 μm haematoxylin and eosin staining was used to identify regions of interest for excision from normal and neoplastic specimens. Right panels: pathologist-identified regions of interest were microdissected from 10 μm sections for RNA purification.

470 miRNAs) with RNA extracted from the specimens displayed in Figure 1.

To evaluate the accuracy of miRNA profiling experiments with formalin-fixed, paraffin-embedded (FFPE) RNA, we compared the miRNA expression results between matched frozen and 1-month-old FFPE normal breast tissues. Duplicates for the frozen RNA samples ($r^2 > 0.98$) and FFPE RNA ($r^2 > 0.97$) were highly concordant with each other ($r^2 > 0.90$) (data not shown) and clustered together during the analysis (Figure 2). Similarly, miRNA profiles of archived normal lobular epithelium, LCIS, and ILC samples provided highly concordant duplicates ($r^2 > 0.979$ in all cases), which clustered together during the analysis. Using a cut-off of $p < 0.02$, the ANOVA analysis identified 85 miRNAs differentially expressed between normal and neoplastic samples. These miRNAs were used for hierarchical clustering of the samples (Euclidean method, Figure 2). Our analysis also revealed that miRNA expression profiles of LCIS and ILC samples, found synchronously in the same patient but obtained from separate archived blocks, clustered together, suggesting a molecular relationship between LCIS and ILC [4,5].

Two groups emerged from the hierarchical clustering (Figure 2), which included six miRNAs highly expressed in normal specimens: hsa-miR-224, hsa-miR-139, hsa-miR-10b, hsa-miR-450, hsa-miR-140, and hsa-miR-365; and six miRNAs expressed at low levels in normal tissue but elevated in LCIS and ILC samples: hsa-miR-375, hsa-miR-182, hsa-miR-425-5p, hsa-miR-183, hsa-miR-196a, and hsa-miR-565 (Figure 2).

Quantitative RT-PCR analyses of hsa-miR-375, -183, and -182 in archived samples

Because miRNA expression analyses revealed that hsa-miR-375 was most differentially expressed in lobular neoplasia, and because hsa-miR-182 and hsa-miR-183 belong to the same miRNA cluster and appeared co-expressed during progression of lobular neoplasia, we selected these three miRNAs for qRT-PCR studies on a larger set of clinical samples ($n = 28$; Table 1). We used two of the profiled specimens (the LCIS synchronous with ILC, and the synchronous ILC) and 26 additional specimens. We established a baseline by measuring the expression of each miRNA in five normal lobular breast epithelium samples and determined

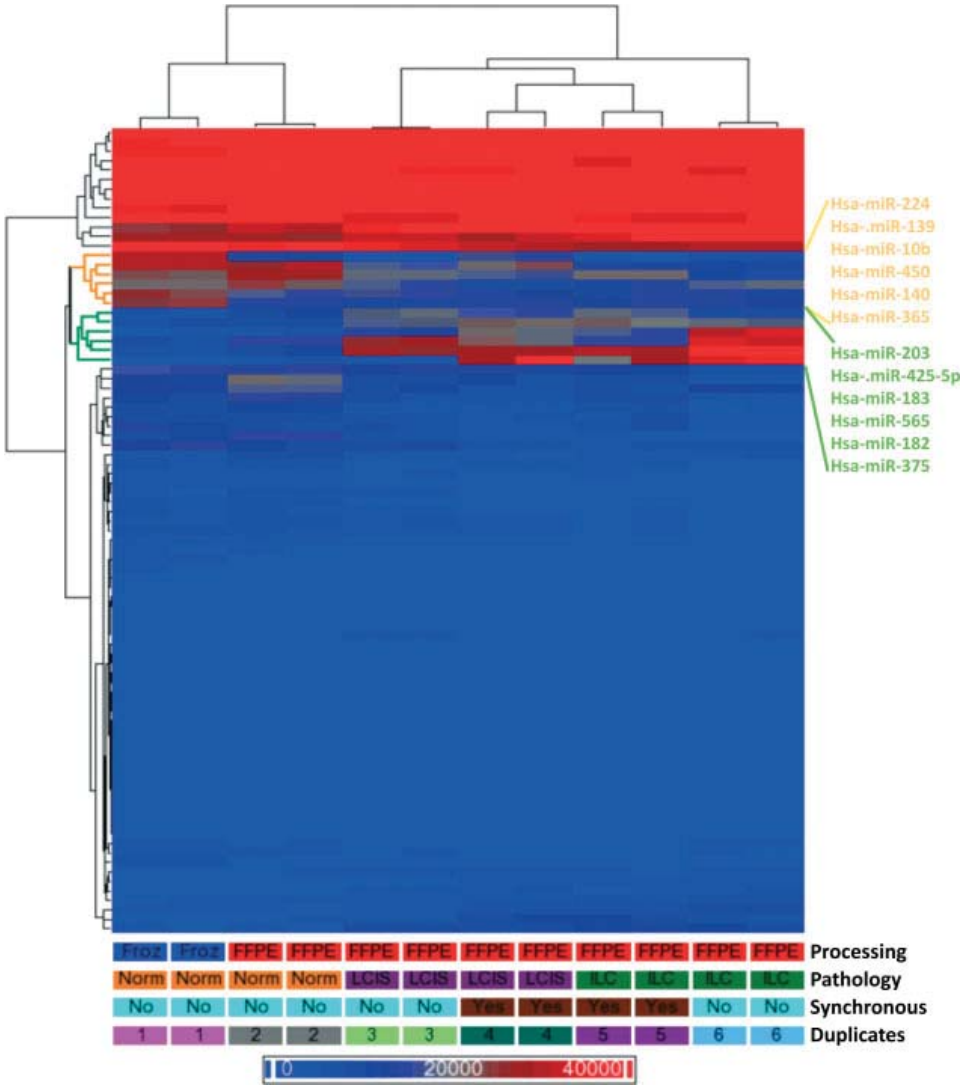

Figure 2. MiRNA profiling of normal, LCIS, and ILC samples reveals a cluster of microRNAs enriched in lobular neoplasia. Euclidean hierarchical clustering of miRNAs demonstrating variable expression between normal and neoplastic samples (ANOVA, $p < 0.02$). A set of six miRNAs up-regulated in normal epithelium: hsa-miR-224, -139, -10b, -450, -140, and -365; and a set of six miRNAs, hsa-miR-203, -425-5p, -183, -565, -182, and -375, enriched in the neoplastic samples.

the level of each miRNA in the neoplastic samples relative to that baseline.

QRT-PCR experiments displayed in Figure 3 demonstrate a trend of increasing expression for hsa-miR-375 ($p < 0.003$), hsa-miR-182 ($p < 0.001$), and hsa-miR-183 ($p < 0.003$) with increasing histological severity of the lesions, with the lowest expression levels in normal lobular specimens and the highest expression levels in ILC specimens. Hsa-miR-182 and hsa-miR-183 displayed similar trends of increased expression, possibly related to their localization in the hsa-miR-183/182/96 cluster [26].

Hsa-miR-375 expression in neoplastic cells

We selected hsa-miR-375 for further *in situ* hybridization (ISH) validation because it displayed the highest expression levels on the Illumina miRNA BeadChips and in qRT-PCR experiments, in comparison with hsa-miR-182 and hsa-miR-183. Our data show that hsa-miR-375 displayed low expression levels in normal samples and in LCIS specimens found alone (without a synchronous ILC), while showing increased expression levels in LCIS and ILC synchronous cases (Figure 3, hsa-miR-375). Increased expression was observed in both histologically high-grade pleiomorphic LCIS cases (Figure 3, hsa-miR-375, first and last bar in the LCIS synch group; LCIS synch1 and LCIS synch8 in Table 1) and the LCIS with necrosis (Figure 3, hsa-miR-375, third bar in the LCIS synch group; LCIS synch3 in Table 1). Although the tissue dissection approach was designed to exclude stromal tissue, it remained possible that high levels of hsa-miR-375 may have originated from infiltrating stromal cells. Thus, we performed ISH experiments with archived specimens to localize and validate

Table 1. Clinical data on archived specimens used for qRT-PCR validations

Case	Age (years)	Clinical finding	Pathology				FFPE storage (years)
Normal 1	40	Calcification	–				1
Normal 2*	50	Calcification	–				2
Normal 3	19	Reduction	–				0.5
Normal 4	53	Reduction	–				0.5
Normal 5	51	Reduction	–				0.5
Case	**Age (years)**	**Clinical finding**	**LCIS nuclear grade**			**Comedo necrosis**	**FFPE storage (years)**
LCIS a1*	50	Calcification	2			Absent	2
LCIS a2	54	Mastectomy	2			Absent	1
LCIS a3	78	Calcification	2			Present	0.5
LCIS a4	66	Mass/fibroadenoma	1			Absent	0.5
LCIS a5	48	Calcification	2			Absent	1
LCIS a6	64	Mass/phyllodes tumour	1			Absent	0.5
LCIS a7	57	Nipple discharge/papilloma	1			Absent	1
Case	**Age (years)**	**Clinical finding**	**LCIS nuclear grade**			**Comedo necrosis**	**FFPE storage (years)**
LCIS synch1†	53	Calcium	3			Present	1
LCIS synch2	51	Mass	2			Absent	1
LCIS synch3	59	Calcium	2			Present	3
LCIS synch4	42	Mass	2			Absent	2
LCIS synch5	73	Mass	2			Absent	1
LCIS synch6	54	Mass	2			Absent	0.5
LCIS synch7	69	Mass	2			Absent	0.5
LCIS synch8	52	Calcium	3			Present	0.5
LCIS synch9			Sample not available				
Case	**Age (years)**	**Clinical finding**	**Size (cm)**	**ER (%+)**	**PR (%+)**	**Axilla lymph nodes**	**FFPE storage (years)**
ILC synch1†	53	Calcium	1.1	> 95%	> 95%	N0 (i+)	1
ILC synch2	51	Mass	3.5	> 95%	> 95%	N0 (i+)	1
ILC synch3	59	Calcium	2.0	N/A	N/A	N1 mi	3
ILC synch4	42	Calcium	1.4	30%	10%	N1 mi	2
ILC synch5	73	Mass	1.5	90%	0%	N0 (i+)	1
ILC synch6	54	Mass	2.9	95%	95%	N0	0.5
ILC synch7	69	Mass	1.5	100%	< 5%	N0	0.5
ILC synch8			Sample not available				
ILC synch9	74	Mass	4.5	90%	60%	N0	0.5

*Specimens obtained from the same patient. LCIS synchronously found with ILC are termed LCIS synch and the ILC counterpart is termed ILC synch. Identical numbers between LCIS synch and ILC synch represent specimens obtained from the same patients (eg LCIS synch1 and ILC synch1 were obtained from the same patient). †Specimens that were also analysed on the Illumina miRNA profiling platform. The size and lymph node status were based on the original tumour. N0 describes lymph nodes without tumour cells; N0 (i+) describes lymph nodes with tumour cells with a size less than 0.2 mm; N1 mi describes lymph nodes with micro-metastases larger than 0.2 mm but smaller than 2 mm.

the expression of hsa-miR-375 (Figure 4). We optimized our *in situ* detection of hsa-miR-375 on human archived pancreas, as pancreatic islets of Langerhans have been reported to express high levels of hsa-miR-375 [27,28]. QRT-PCR with RNA extracted from a 1-year-old FFPE pancreas revealed that hsa-miR-375 expression was 1078-fold higher than in normal breast epithelium (data not shown). We used H&E staining to distinguish the endocrine islets of Langerhans (Figure 4A, see arrowheads, light staining) from the exocrine pancreas (darker staining). ISH detection of hsa-miR-375 revealed robust expression in the islets of Langerhans (Figure 4B, hsa-miR-375, purple stain) compared with the surrounding exocrine tissue. No staining was observed with the negative control scrambled probe (Figure 4B, scrambled). The expression pattern of hsa-miR-375 in the pancreas validated our detection assay. We applied the same ISH procedure to archived breast specimens (Figure 4C). The scrambled miRNA probe resulted in no staining (Figure 4C, left column), while ISH detection of hsa-miR-375 revealed weak expression in normal breast epithelium and LCIS lesions found alone, but the highest expression levels within LCIS and ILC lesions found synchronously. These data support the differential expression of hsa-miR-375 observed by high-throughput miRNA profiling (Figure 2) and qRT-PCR experiments (Figure 3), and confirm that hsa-miR-375 is primarily expressed in the neoplastic cells of these specimens. Similar ISH detection data were obtained for hsa-miR-182, the second highest expressed miRNA after hsa-miR-375 (see Supporting information, Supplementary Figure 1).

Hsa-miR-375 expression disrupts mammary acinar morphogenesis

Analysis of miRNA expression in a larger set of clinical samples would be necessary to determine whether the expression levels of hsa-miR-375, hsa-miR-182, and hsa-miR-183 have prognostic utility but also to help identify other up-regulated and down-regulated miRNAs which may correlate with lobular neoplasia progression. However, because increased expression of hsa-miR-375, in MCF-7 cells, has been associated

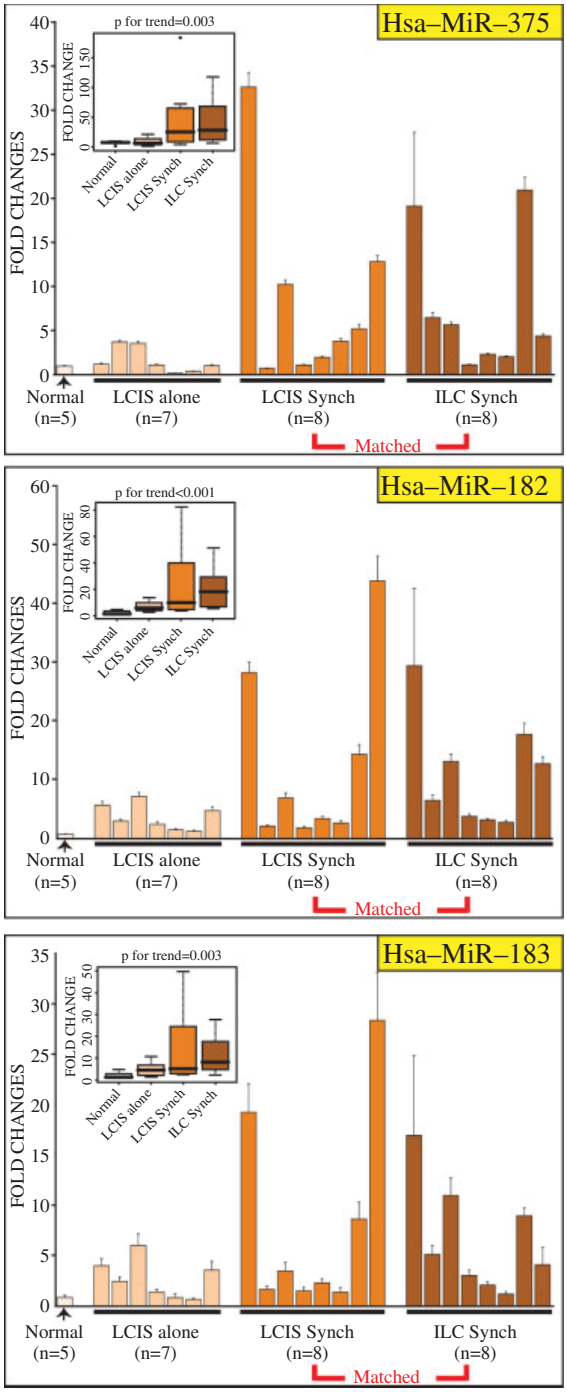

Figure 3. Quantitative RT-PCR analysis of hsa-miR-375, hsa-miR-183, and hsa-miR-182 in lobular neoplasia. The quantification was performed using the $\Delta\Delta C_t$ method described in the Materials and methods section. The coloured bar-graphs represent miRNA expression measured in fold change [$2^{(\Delta Ct\ normal - \Delta Ct\ LCIS\ sample)}$], by comparison with normal lobular cells [average of five samples ($n = 5$)]. The endogenous controls RNU44 and RNU6B [mean of the comparative threshold (C_t) between both controls] were used to normalize miRNA expression in each specimen. Insets: box and whisker plots showing the distribution of the expression levels of each miRNA between normal ($n = 5$), LCIS alone ($n = 7$), LCIS synchronous with ILC ($n = 8$), and the synchronous ILC samples ($n = 8$) plotted as fold change. The p value represents the test for trend of expression.

with increased proliferation [29], and its expression is found at its highest levels in LCIS synchronous with ILC (Figures 2–4), we hypothesized that increased expression of hsa-miR-375 may contribute to the progression of lobular breast neoplasia. We used the MCF-10A model of mammary acinar morphogenesis to test the effect of increased expression of hsa-miR-375. When this cell line is cultured within a reconstituted basement membrane (Matrigel), it forms small colonies, which over a period of time develop the central lumen and apicobasal polarity that characterize human mammary epithelial cells *in vivo*. Experimental overexpression of various oncogenes in MCF-10A cells, in 3D culture, leads to phenotypes including hyperplastic growth, failure of apoptosis, and the formation of multi-lobular colonies [30]. To determine whether increased expression of hsa-miR-375 may affect the maintenance of correct breast tissue polarity in 3D culture, we used lentiviral expression to stably express hsa-miR-375 in MCF-10A cells. QRT-PCR analysis (Figure 5A) evaluated the levels of hsa-miR-375 in MCF-10A^{ctrl} cells and MCF-10A$^{hsa-miR-375}$ cells by comparison with hsa-miR-375 expression levels in normal breast epithelium and the LCIS synchronous with ILC case that displayed the highest expression (Figure 3, LCIS synch1). The qRT-PCR results demonstrate that hsa-miR-375 is expressed at low levels in the MCF-10A^{ctrl} cells and at high levels in MCF-10A$^{hsa-miR-375}$ cells, comparable to the levels detected in the LCIS synchronous with ILC (Figure 3, see hsa-miR-375, LCIS synch1).

Pools of infected cells were selected using puromycin, and analysis of co-expressed RFP was performed prior to each experiment to confirm that the majority of cells in the pool had retained the lentivirus (Figure 5B). MCF-10A cells were seeded singly on top of Matrigel [24,28] and allowed to form colonies for 4 weeks (Figure 5C, left). MCF-10A cells expressing hsa-miR-375 formed larger and more misshapen colonies, and the relative difference in cross-sectional area was highly statistically significant (Figure 5C, right). In addition, hsa-miR-375-expressing colonies cleared significantly fewer cells from the centre of the colonies compared with the vector control. We further analysed the status of tissue polarity in these structures, using α6-integrin as a marker of basal tissue polarity. In MCF-10A^{ctrl} cells, α6-integrin was localized at the basal surface of these cells, while this organization was completely disrupted in the MCF-10A$^{hsa-miR-375}$ colonies. These data suggest that increasing hsa-miR-375 expression to the levels found in human lobular neoplasia specimens may alter the ability of human breast epithelial cells to establish and maintain appropriate tissue organization.

Discussion

We report the first study to identify a number of up-regulated miRNAs during progression of lobular

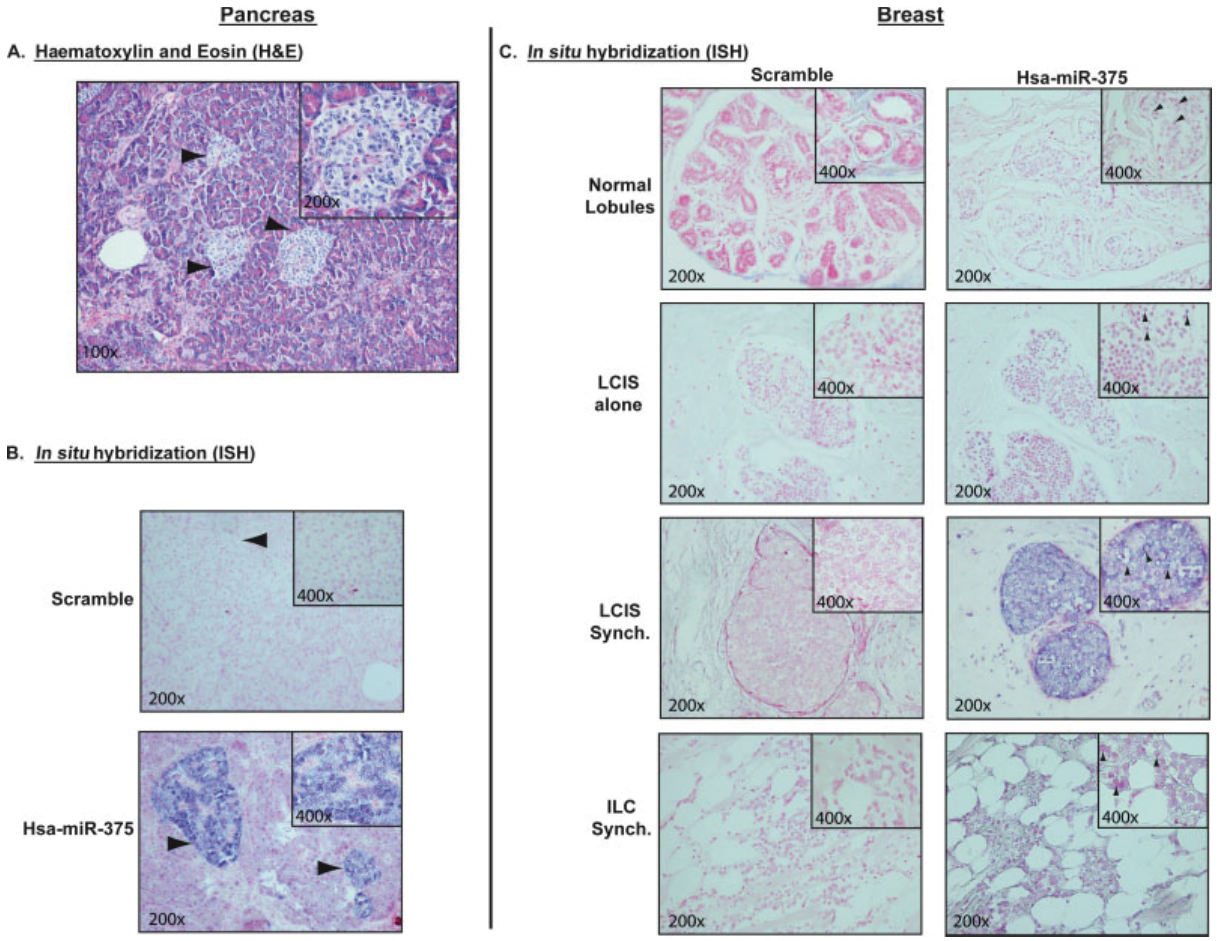

Figure 4. *In situ* hybridization analysis of hsa-mir-375 expression during lobular neoplastic progression. (A) Haematoxylin and eosin analysis of archived pancreas. The picture shows the presence of several islets of Langerhans (original magnification 200×, see arrows), with one of them enlarged for morphology analysis (original magnification 400×). (B) *In situ* hybridization detection of hsa-miR-375 in islets of Langerhans used as a positive control for the protocol used to detect hsa-miR-375 (reference). The scramble panels show light staining of the nuclei (red nuclear stain), and the expression of hsa-miR-375 is detected specifically in islets of Langerhans (blue/purple stain), with a light purple stain in surrounding cells. (C) *In situ* hybridization detection of hsa-miR-375 in normal lobular cells and lobular neoplasia. The left column displays the negative control (scramble probe) and the right column the detection of hsa-miR-375. From top to bottom, hsa-miR-375 can be detected very weakly in the nuclei of normal lobular cells and LCIS alone (LCIS alone case 2 in qRT-PCR of hsa-miR-375 in Figure 3), see arrowheads in 400× panels, respectively. High expression of hsa-miR-375 can be detected in the cytoplasm of LCIS synch cells (LCIS synch case 1 in qRT-PCR of hsa-miR-375 in Figure 3). A weaker cytoplasmic stain is visible in ILC synch cells (ILC synch case 1 in qRT-PCR of hsa-miR-375 in Figure 3). For each individual tissue, the nucleolar U6-RNA was tested as a second positive control (data not shown).

neoplasia. When we transduced and overexpressed hsa-miR-375, one of the miRNAs up-regulated in lobular neoplasia, in MCF-10A cells, a model of human mammary acinar morphogenesis, we found that it led to the production of larger dysmorphic colonies with filled lumens and substantial perturbations in tissue polarity, phenotypes recapitulating, at least in part, the ones observed during lobular neoplasia. This study is the first to show that ectopic expression of a single miRNA can interfere with the organization of human breast epithelial cells in a 3D context.

MiRNAs are key regulators of gene expression, and abnormal expression of these molecules has been shown to correlate with the progression of many human cancers [14]. MiRNA expression studies of human breast tumours have shown that these molecules can be utilized as prognostic markers [19,31]. Although the number of specimens analysed here was too small to develop a prognostic signature, our study strongly indicates that miRNA expression analysis in larger cohorts may allow the development and validation of prognostic or predictive signatures in lobular neoplasia.

Our qRT-PCR analyses focused on three up-regulated miRNAs, hsa-miR-182, hsa-miR-183, and hsa-miR-375, and showed that expression changes follow transition from normal, to pre-invasive, to invasive lobular carcinomas. Our results show that up-regulation of hsa-miR-182 and hsa-miR-183 is detected in LCIS lesions synchronous with ILC. Up-regulation of both hsa-miR-182 and hsa-miR-183 has been described in breast cancer cells and recently in DCIS, when compared with normal breast epithelium, supporting

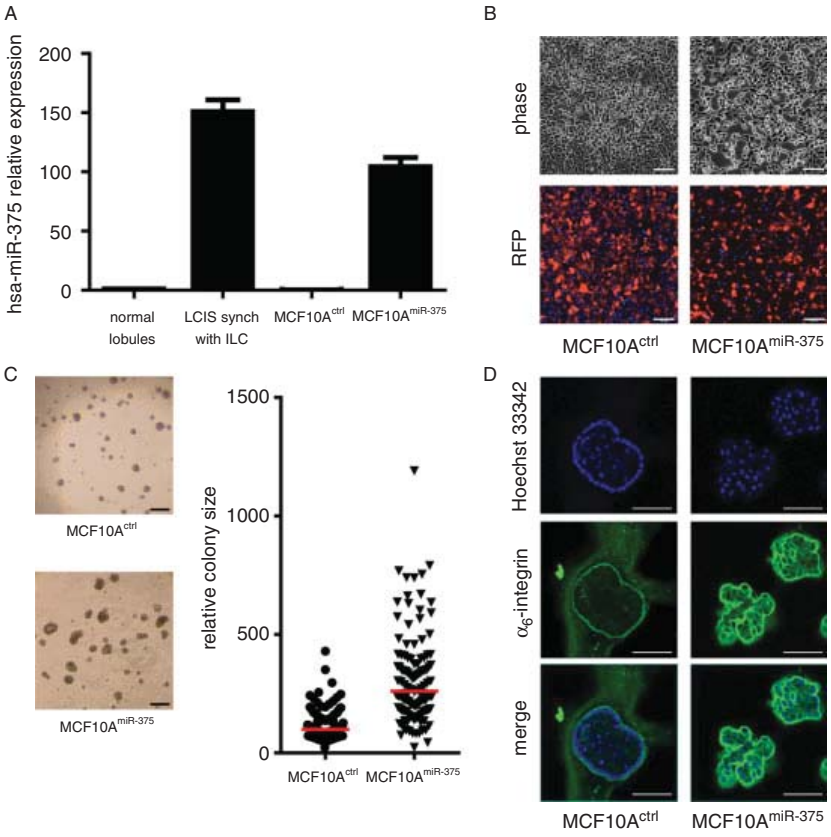

Figure 5. Hsa-mir-375 expression disrupts mammary epithelial polarity. (A) Quantitative RT-PCR of hsa-miR-375 expression in LCIS synch case 1 (Figure 3, hsa-miR-375 graph, first bar in LCIS synch group) and MCF-10A$^{hsa-miR-375}$, and their respective normal controls. (B) 2D culture of MCF-10A^{ctrl} (empty lentiviral vector) and MCF-10A$^{hsa-mir-375}$ cells (scale bar = 200 mm). Red fluorescent protein expression indicates stable infection by lentiviral vectors. (C) 3D culture in Matrigel and colony size analysis (scale bar = 100 mm). (D) Immunofluorescence analysis of single colonies from MCF-10A^{ctrl} and MCF-10A$^{hsa-miR-375}$ in 3D cultures using Hoechst 33342 (nuclei) and α6-integrin, a marker of mammary epithelial polarity (scale bar = 50 mm).

the idea that these two miRNAs may play important roles in the development of breast cancer [32]. Increased expression of hsa-miR-182 in MCF-7 cells has been linked with down-regulation of FOXO1, a transcription factor orchestrating genes involved in apoptotic response, cell cycle checkpoints, and cellular metabolism [33]. Using MCF-7 cells, Hannafon *et al* [32] recently identified four additional targets (CBX7, DOK4, NMT2, and EGR1), and their results suggest that hsa-miR-182 may also be indirectly involved in down-regulation of E-cadherin expression in DCIS, an interesting finding as loss of E-cadherin is a hallmark of LCIS. Although our analysis of LCIS and the analysis of DCIS have converged on similar miRNA dysregulations, it is important to note that gene expression patterns may differ between DCIS and LCIS, as gene expression patterns differ in their respective invasive cancers, thus providing distinct gene targets involved in different pathways [32,34]. Our data show that hsa-miR-182 and hsa-miR-183 are co-dysregulated in the same LCIS samples. These two miRNAs are clustered with hsa-miR-96 on chromosome 7q32.2, a region frequently amplified in melanoma [35]. Co-dysregulation of hsa-miR-182 and hsa-miR-183 has also been described in prostate and colon cancers, but their co-expression in normal tissue has been associated with development of the inner ear, suggesting common transcriptional regulation mechanisms for these miRNAs [36–38]. Together, decrease of cellular adhesion (loss of E-cadherin), decrease of apoptosis, disruption of cell-cycle checkpoints, and cellular metabolism suggest that dysregulation of hsa-miR-182 and hsa-miR-183 may play important roles in breast cancer, and our results suggest that these miRNAs may play important roles in the progression of pre-invasive lesions towards invasive cancers.

Strong up-regulation of hsa-miR-375 in LCIS lesions synchronous with ILC and high expression in the synchronous ILC cells suggest an important role for this miRNA in the transition from pre-invasive to invasive lobular cancer cells. The dysregulated expression of hsa-miR-375 has been reported in at least five different human cancers, including gastric [39,40], head and neck [41], and liver cancers [42,43], where the expression of hsa-miR-375 is down-regulated by comparison with normal tissues, and lung [44] and breast cancers [29], where hsa-miR-375 expression is up-regulated. The study of De Souza Rocha Simonini *et al* [29], on

the ER-positive (ER+) MCF-7 breast cancer cell line, has suggested that increased expression of hsa-miR-375 may play a role in the progression of ER+ breast tumours by indirectly increasing ERα expression and thus cellular proliferation, an interesting observation in the context of invasive lobular carcinomas as 93.1% of these cancers are ER+. As there are no culture models of ER+ non-malignant breast epithelial cells, we evaluated the impact of increased hsa-miR-375 expression in the ER-negative (ER−) MCF-10A cell line. In a 3D context, upon up-regulation of hsa-miR-375, these cells formed larger colonies with disrupted tissue organization and increased proliferation. These data suggest that ERα is not the only key molecule affected by hsa-miR-375 during tumourigenesis and that additional key targets, involved in the 3D architecture of breast epithelium, remain to be discovered.

Analysis of *hsa-miR-375* null mice has demonstrated that hsa-miR-375 plays important roles in the development of normal pancreatic endocrine cell mass in the postnatal period, and has further demonstrated its role in the maintenance of glucose homeostasis [27,28]. Gene expression analysis of *hsa-miR-375*-null islets, from KO mice, revealed that several hundred genes were up-regulated in these cells. Using target prediction and RT-PCR analysis, Poy *et al* [28] validated 20 targets, which included genes with roles in the p53 pathway, MAPK signalling, apoptosis, and cellular adhesion, several of which have been reported to play important roles in breast cancer.

Research in lobular cancer requires the use of cell line models. We tested the MDA-MB-134 cell line, which is considered to be of lobular origin, for the expression of hsa-miR-375 and found that it was highly elevated (data not shown), compared with that in MCF-10A and MCF-7 cells [45,46]. The MDA-MB-134 cells may be useful for the identification of hsa-miR-375 targets. However, the MCF-10A cell line, a model for human mammary acinar morphogenesis, recapitulates aspects of the organization of the terminal duct lobule unit (TDLU) and represents an interesting study model for analysis of the capability of candidate genes to alter mammary phenotypes and, more particularly, the contribution of miRNAs, as we have shown in our study.

Molecular profiling of breast lesions associated with a high risk of subsequent breast cancer development represents a potential approach to developing strategies for reducing the burden of this disease. In this regard, women with lobular intra-epithelial neoplasia are of interest, given the increased risk of subsequent development of invasive breast cancer, which persists indefinitely after initial diagnosis [47]. Considering that LCIS lesions with similar histological appearance can have different outcomes, understanding the underlying molecular differences between lesions may help in predicting their behaviour. The identification of biomarkers in early lesions, which are predictive of the future clinical course of the disease, may help to identify women at high risk of progression who may benefit from surgery, chemoprevention with a selective oestrogen receptor modulator, and/or increased monitoring, and conversely, may reduce the overtreatment of patients whose indolent disease is less likely to progress to an invasive carcinoma.

Our study demonstrates that retrospective analysis of archived benign and pre-invasive breast lesions, from large cohorts with extensive follow-up, has potential to help identify and develop predictors for breast lesions likely to progress to invasive disease [30,48,49].

Acknowledgment

We wish to thank Dr Sunhee Lee for providing access to microscopy and photography for pictures of the tissues presented in this article. We thank Dr Michael Prystowsky and Dr Qiulu Pan for providing access to the Illumina® technology in the molecular pathology laboratories, and Michael Ronan for his technical advice and training on the Illumina® platform. For financial support, we thank Susan G Komen for the Cure (KG100888 to PK and KG091136 to PK and OG).

Author contribution statement

OL, TR, SF, and NS conceived the study. SF and NS identified suitable specimens. OL and CL isolated RNA, and performed expression studies (GC provided support during miRNA profiling experiments) and qRT-PCR experiments. OL, PK, and TW analysed the expression data. AR, LS, and OL performed and analysed the *in situ* hybridization experiments. PAR generated the MCF-10A derivatives. OG and PK designed and performed the 3D culture assays. OL and PK wrote the manuscript and all the authors approved the final manuscript.

References

1. Biglia N, Mariani L, Sgro L, *et al*. Increased incidence of lobular breast cancer in women treated with hormone replacement therapy: implications for diagnosis, surgical and medical treatment. *Endocr Relat Cancer* 2007; **14**: 549–567.
2. Wasif N, Maggard MA, Ko CY, *et al*. Invasive lobular vs. ductal breast cancer: a stage-matched comparison of outcomes. *Ann Surg Oncol* 2010; **17**: 1862–1869.
3. Simpson PT, Reis-Filho JS, Gale T, *et al*. Molecular evolution of breast cancer. *J Pathol* 2005; **205**: 248–254.
4. Aulmann S, Penzel R, Longerich T, *et al*. Clonality of lobular carcinoma *in situ* (LCIS) and metachronous invasive breast cancer. *Breast Cancer Res Treat* 2008; **107**: 331–335.
5. Hwang ES, Nyante SJ, Yi Chen Y, *et al*. Clonality of lobular carcinoma *in situ* and synchronous invasive lobular carcinoma. *Cancer* 2004; **100**: 2562–2572.
6. Morandi L, Marucci G, Foschini MP, *et al*. Genetic similarities and differences between lobular *in situ* neoplasia (LN) and invasive lobular carcinoma of the breast. *Virchows Arch* 2006; **449**: 14–23.

7. Vos CB, Cleton-Jansen AM, Berx G, *et al*. E-cadherin inactivation in lobular carcinoma *in situ* of the breast: an early event in tumorigenesis. *Br J Cancer* 1997; **76**: 1131–1133.
8. O'Malley FP. Lobular neoplasia: morphology, biological potential and management in core biopsies. *Mod Pathol* 2010; **23**(Suppl 2): S14–S25.
9. Sullivan ME, Khan SA, Sullu Y, *et al*. Lobular carcinoma *in situ* variants in breast cores: potential for misdiagnosis, upgrade rates at surgical excision, and practical implications. *Arch Pathol Lab Med* 2010; **134**: 1024–1028.
10. Venkitaraman R. Lobular neoplasia of the breast. *Breast J* 2010; **16**: 519–528.
11. Mastracci TL, Tjan S, Bane AL, *et al*. E-cadherin alterations in atypical lobular hyperplasia and lobular carcinoma *in situ* of the breast. *Mod Pathol* 2005; **18**: 741–751.
12. Rosen PP. Microglandular adenosis. A benign lesion simulating invasive mammary carcinoma. *Am J Surg Pathol* 1983; **7**: 137–144.
13. Rakha EA, Ellis IO. Lobular breast carcinoma and its variants. *Semin Diagn Pathol* 2010; **27**: 49–61.
14. Calin GA, Sevignani C, Dumitru CD, *et al*. Human microRNA genes are frequently located at fragile sites and genomic regions involved in cancers. *Proc Natl Acad Sci U S A* 2004; **101**: 2999–3004.
15. Sotiropoulou G, Pampalakis G, Lianidou E, *et al*. Emerging roles of microRNAs as molecular switches in the integrated circuit of the cancer cell. *RNA* 2009; **15**: 1443–1461.
16. Zeng Y. Principles of micro-RNA production and maturation. *Oncogene* 2006; **25**: 6156–6162.
17. Lewis BP, Burge CB, Bartel DP. Conserved seed pairing, often flanked by adenosines, indicates that thousands of human genes are microRNA targets. *Cell* 2005; **120**: 15–20.
18. Zhang B, Pan X, Cobb GP, *et al*. microRNAs as oncogenes and tumor suppressors. *Dev Biol* 2007; **302**: 1–12.
19. Heneghan HM, Miller N, Lowery AJ, *et al*. MicroRNAs as novel biomarkers for breast cancer. *J Oncol* 2009; **2009**: 950201.
20. Loudig O, Milova E, Brandwein-Gensler M, *et al*. Molecular restoration of archived transcriptional profiles by complementary-template reverse-transcription (CT-RT). *Nucleic Acids Res* 2007; **35**: e94.
21. Chen J, Lozach J, Garcia EW, *et al*. Highly sensitive and specific microRNA expression profiling using BeadArray technology. *Nucleic Acids Res* 2008; **36**: e87.
22. Jorgensen S, Baker A, Moller S, *et al*. Robust one-day *in situ* hybridization protocol for detection of microRNAs in paraffin samples using LNA probes. *Methods* 2010; **52**: 375–381.
23. Selvin S. *Statistical Analysis for Epidemiologic Data* (2nd edn). Oxford University Press: New York, 1996; 228.
24. Debnath J, Muthuswamy SK, Brugge JS. Morphogenesis and oncogenesis of MCF-10A mammary epithelial acini grown in three-dimensional basement membrane cultures. *Methods* 2003; **30**: 256–268.
25. Neter J, Wasserman W. *Applied Linear Statistical Models: Regression, Analysis of variance, and Experimental Design*. Richard D Irwin, Inc: Homewood, IL, 1974; 319.
26. Li H, Kloosterman W, Fekete DM. MicroRNA-183 family members regulate sensorineural fates in the inner ear. *J Neurosci* 2010; **30**: 3254–3263.
27. Poy MN, Eliasson L, Krutzfeldt J, *et al*. A pancreatic islet-specific microRNA regulates insulin secretion. *Nature* 2004; **432**: 226–230.
28. Poy MN, Hausser J, Trajkovski M, *et al*. miR-375 maintains normal pancreatic alpha- and beta-cell mass. *Proc Natl Acad Sci U S A* 2009; **106**: 5813–5818.
29. de Souza Rocha Simonini P, Breiling A, Gupta N, *et al*. Epigenetically deregulated microRNA-375 is involved in a positive feedback loop with estrogen receptor alpha in breast cancer cells. *Cancer Res* 2010; **70**: 9175–9184.
30. Debnath J, Brugge JS. Modelling glandular epithelial cancers in three-dimensional cultures. *Nature Rev Cancer* 2005; **5**: 675–688.
31. Iorio MV, Croce CM. MicroRNAs in cancer: small molecules with a huge impact. *J Clin Oncol* 2009; **27**: 5848–5856.
32. Hannafon BN, Sebastiani P, de Las Morenas A, *et al*. Expression of microRNAs and their gene targets are dysregulated in preinvasive breast cancer. *Breast Cancer Res* 2011; **13**: R24.
33. Guttilla IK, White BA. Coordinate regulation of FOXO1 by miR-27a, miR-96, and miR-182 in breast cancer cells. *J Biol Chem* 2009; **284**: 23204–23216.
34. Turashvili G, Bouchal J, Baumforth K, *et al*. Novel markers for differentiation of lobular and ductal invasive breast carcinomas by laser microdissection of microarray analysis. *BMC Cancer* 2007; **7**: 55.
35. Segura MF, Hanniford D, Menendez S, *et al*. Aberrant miR-182 expression promotes melanoma metastasis by repressing FOXO3 and microphthalmia-associated transcription factor. *Proc Natl Acad Sci U S A* 2009; **106**: 1814–1819.
36. Schaefer A, Jung M, Mollekopf HJ, *et al*. Diagnostic and prognostic implications of microRNA profiling in prostate cancer. *Int J Cancer* 2010; **126**: 166–176.
37. Sarver AL, French AJ, Borralho PM, *et al*. Human colon cancer profiles show differential microRNA expression depending on mismatch repair status and are characteristic of undifferentiated proliferative states. *BMC Cancer* 2009; **9**: 401.
38. Sacheli R, Nguyen L, Borgs L, *et al*. Expression patterns of miR-96, miR-182 and miR-183 in the development inner ear. *Gene Expr Patterns* 2009; **9**: 364–370.
39. Ding L, Xu Y, Zhang W, *et al*. MiR-375 frequently downregulated in gastric cancer inhibits cell proliferation by targeting JAK2. *Cell Res* 2010; **20**: 784–793.
40. Tsukamoto Y, Nakada C, Noguchi T, *et al*. MicroRNA-375 is downregulated in gastric carcinomas and regulates cell survival by targeting PDK1 and 14-3-3zeta. *Cancer Res* 2010; **70**: 2339–2349.
41. Avissar M, Christensen BC, Kelsey KT, *et al*. MicroRNA expression ratio is predictive of head and neck squamous cell carcinoma. *Clin Cancer Res* 2009; **15**: 2850–2855.
42. Ladeiro Y, Couchy G, Balabaud C, *et al*. MicroRNA profiling in hepatocellular tumors is associated with clinical features and oncogene/tumor suppressor gene mutations. *Hepatology* 2008; **47**: 1955–1963.
43. Liu AM, Poon RT, Luk JM. MicroRNA-375 targets hippo-signalling effector YAP in liver cancer and inhibits tumor properties. *Biochem Biophys Res Commun* 2010; **394**: 623.
44. Zhang H, Mishra A, Chintagari NR, *et al*. Micro-RNA-375 inhibits lung surfactant secretion by altering cytoskeleton reorganization. *IUBMB Life* 2010; **62**: 78–83.
45. Reis-Filho JS, Simpson PT, Turner NC, *et al*. FGFR1 emerges as a potential therapeutic target for lobular breast carcinomas. *Clin Cancer Res* 2006; **12**: 6652–6662.
46. Riggins RB, Lan JP, Zhu Y, *et al*. ERRgamma mediates tamoxifen resistance in novel models of invasive lobular breast cancer. *Cancer Res* 2008; **68**: 8908–8917.
47. Bodian CA, Perzin KH, Lattes R. Lobular neoplasia. Long term risk of breast cancer and relation to other factors. *Cancer* 1996; **78**: 1024–1034.
48. Silvera SA, Rohan TE. Benign proliferative epithelial disorders of the breast: a review of the epidemiologic evidence. *Breast Cancer Res Treat* 2008; **110**: 397–409.
49. Kabat GC, Jones JG, Olson N, *et al*. Risk factors for breast cancer in women biopsied for benign breast disease: a nested case–control study. *Cancer Epidemiol* 2010; **34**: 34–39.

SUPPORTING INFORMATION ON THE INTERNET

The following supporting information may be found in the online version of this article.

Figure S1. *In situ* hybridization analysis of hsa-miR-182 expression during lobular neoplastic progression.